Materials Advances

ROYAL SOCIETY OF CHEMISTRY

PAPER

View Article Online
View Journal | View Issue

Cite this: *Mater. Adv.*, 2022, 3, 3952

Wool fabrics decorated with carbon-based conductive ink for low-voltage heaters†

Hamid Souri *[a] and Debes Bhattacharyya[b]

Received 22nd October 2021,
Accepted 19th March 2022

DOI: 10.1039/d1ma00981h

rsc.li/materials-advances

Smart textiles have extensively progressed in recent years and have expanded the potential scope and market of textiles, especially in areas of sensing, energy storage and heating. A great opportunity still exists to develop heaters based on natural fibre-based fabrics that are soft, light weight, and biodegradable. In this study, a simple, environmentally friendly, and scalable process to prepare highly conductive wool fabrics (CWFs) is reported. This multi-step process consists of stir coating and dip coating techniques using highly conductive ink based on graphene nanoplatelets (GNPs) and carbon black (CB) particles, followed by the cold-pressing process. Time-dependent temperature profiles and heat distribution analysis of the CWFs showed superior electrothermal performance to the heaters reported in the literature, reaching a surface temperature of more than 230 °C with a low applied voltage of 4.5 V (or an equivalent input power of ~7.2 W). To demonstrate their potential application, the concept of a sandwich-structured and large size heating device was designed and the device was fabricated using a 3 × 3 array of CWFs.

1. Introduction

Newly developed smart textiles with interesting features such as softness, light weight and biodegradability have been greatly researched in the past few years.[1,2] Such features are well satisfied by taking advantage of natural based fabrics.[3] Among several types of natural based fabrics, cotton has been mostly used due to its natural abundance, economic processability, mechanical properties and softness.[4] Different coating techniques and carbonization processes have been mainly employed to produce conductive natural materials for a wide range of applications. Coating techniques such as dip coating,[5–7] electrophoretic deposition (EPD),[8] spray coating[9] and ultrasonication techniques[4,10] have been reported for the preparation of conductive natural materials with the incorporation of conductive particles, such as graphene and its derivatives,[11–14] carbon nanotubes (CNTs),[15–17] carbon black (CB)[18] and metallic particles.[19–21]

Smart textiles acting as heaters have been researched in the past in which they have been mostly based on conductive cotton fabrics.[4,9,19,22–30] For instance, Rahman *et al.* (2015) developed a heater based on cotton fabric decorated with MWCNTs with a maximum surface temperature of 84 °C at a high applied voltage (60 V).[25] In another research study, cotton fabric coated by PEDOT:PSS Joule heated at an applied voltage of 12 V exhibited a maximum surface temperature of 99.6 °C.[26] In another study, a flexible heater based on cotton fabric coated by SWCNTs showed a maximum surface temperature of 45 °C with an input voltage of 40 V.[30] However, to the best of the authors' knowledge, the fabrication of low-voltage heaters based on conductive wool fabrics (CWFs), as cost-effective, biodegradable, light weight and abundant natural materials, and the concept of using such heaters for a large size heating device have been rarely explored in the literature. In general, wool has the advantages of extreme durability, comfort, low flammability, and great water-resistance properties compared to some of the other widely used natural materials such as cotton.[4,7,31] According to our previous study,[4] CWFs have shown excellent thermal stability in the working temperature range of the heaters. These characteristics make wool a suitable candidate as a substrate for heaters.

In the present study, low-voltage heaters by using wool fabrics coated with conductive ink containing a hybrid of graphene nanoplatelets (GNPs) and CB particles are introduced. The fabrication of the CWFs was performed following our previously reported procedure,[7,32] with further modification to minimize the surface cracks within the percolated networks of coated particles after drying. This modification was found to be effective in achieving a more uniform surface temperature on the heaters and the absence of hotspots on their surfaces. The concept of a large size and sandwich-structured heating device

[a] *RaM Group, Faculty of Electrical Engineering, Mathematics and Computer Science, University of Twente, 7500 AE, Enschede, The Netherlands.*
E-mail: souri6889@gmail.com
[b] *Centre for Advanced Composite Materials, Department of Mechanical Engineering, The University of Auckland, 1142, Auckland, New Zealand*

† Electronic supplementary information (ESI) available. See DOI: 10.1039/d1ma00981h

based on a 3 × 3 array of CWFs with a large surface area was designed and the device was fabricated. In order to minimize the input working voltage (or input power) of the concept heating device, a 3 × 3 array of highly conductive CWFs with small size (25 mm × 20 mm) was utilized. The results related to the electro-thermal properties of CWFs as well as the concept heating device showed that CWFs could show potential for application in large size heating devices for warming up and de-icing complex surfaces.

2. Experimental section

2.1 Preparation of materials

Plain weave wool fabric with a measured thickness of ~0.7 ± 0.06 mm, a measured yarn diameter of ~509.7 ± 34.1 μm, a measured fibre diameter of ~49.8 ± 4.6 μm and an areal density of ~0.38 kg m^{-2} was locally purchased as a product of Inter-weave Ltd, New Zealand, and was used as a soft, durable and lightweight textile, suitable for the fabrication of heaters. Graphene nanoplatelets, with 5 nm thickness and 5 μm width, and CB, with an average particle size of 30 nm, were purchased from EMFUTUR, Spain and Orion Engineered Carbons GmbH (formerly known as Degussa), Germany, respectively. According to the manufacturer's catalogue, GNPs (EM-P-G750-50g) have a specific surface area of 700–800 m^2 g^{-1} and a purity of 91% and CB particles (Printex® XE 2-B) have a bulk density of 100–400 kg m^{-3}. They were dispersed in DI water, as an eco-friendly solvent, using a surfactant (sodium dodecylbenzenesulfonate (SDBS), Sigma-Aldrich). SDBS was found to be an effective surfactant in dispersing hybrid carbon particles in DI water and achieving high electrical conductivity as a result of the coating process in accordance with our previous studies.[4,7,8,10] The two parts of the highly elastic elastomer, Ecoflex 0030 (Smooth-On Inc., The USA), were locally purchased from Fibreglass shop, New Zealand.

2.2 Fabrication of CWFs using the modified dip coating technique

The preparation of highly conductive ink is schematically depicted in Fig. 1a, following our previously reported procedure.[4,7,8,10] In brief, 3 g of both GNPs and CB particles were added to 75 ml of DI water and bath-sonicated for 30 min. Next, SDBS (6 g) was added to the mixture and stirred for 4 h at

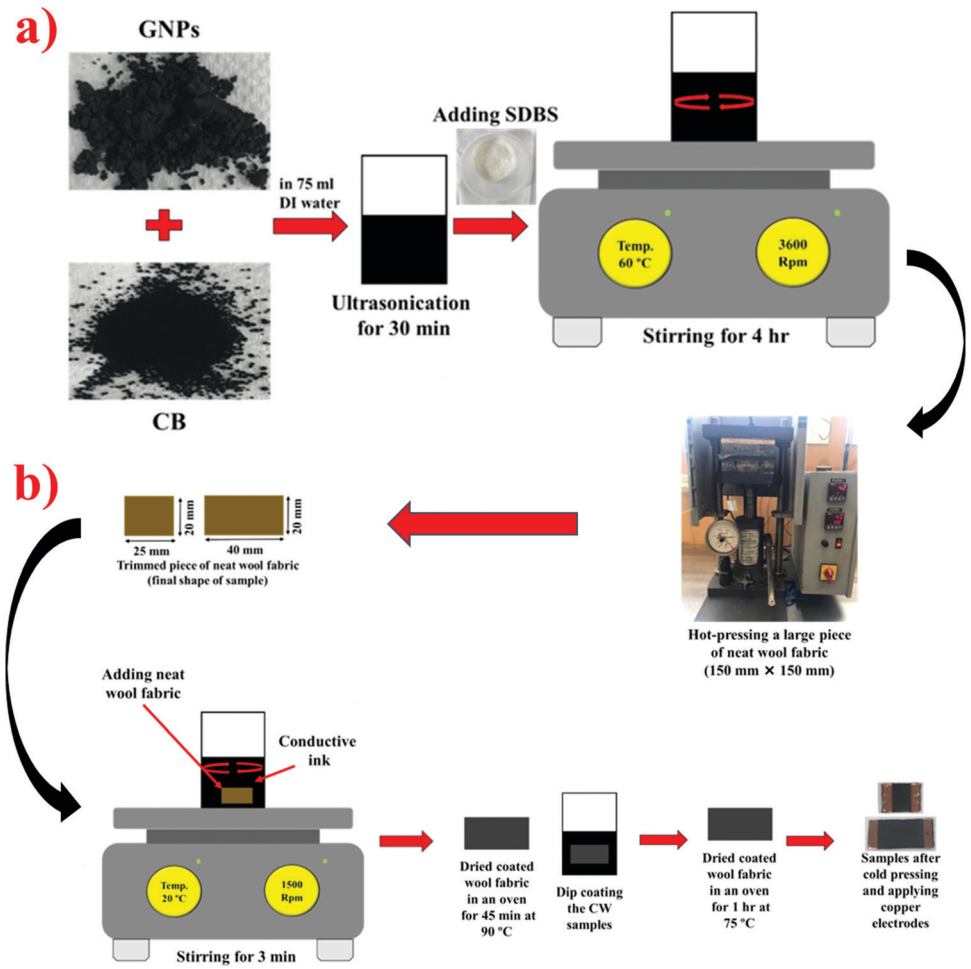

Fig. 1 (a) Schematic illustration of the preparation of conductive ink based on GNPs and CB particles in DI water; (b) fabrication process of CWFs using the prepared conductive ink in three steps.

60 °C following our previously reported procedure.[4,7,8,10] To fabricate CWFs, large wool fabric pieces (150 mm × 150 mm) were hot-pressed using a hydraulic press at 100 °C and 20 000 lb of applied load for 10 min (Fig. 1b). They were trimmed to smaller pieces (45 mm × 20 mm and 25 mm × 20 mm for heaters and 80 mm × 20 mm for measuring electrical conductivity) after cooling; each piece was then introduced to the conductive ink and coated for 3 min by magnetic stirring at 1500 rpm, Fig. 1b. Finally, the CWFs were removed from the conductive ink, placed on a glass substrate and fully dried in an oven at 90 °C for 45 min. After drying, a second coating cycle was conducted by dip coating the CWFs into the identical conductive ink. The wet samples were dried on the glass substrate at 75 °C for 1 h in the same oven. The second coating cycle was carried out to decrease the level of initial resistance of the CWFs, as suggested in previous studies.[33–35] In the next step, the samples were compressed using a cold press under 20 000 lb of applied load for 20 s while copper tape electrodes were placed on each side of CWF heaters. The cold pressing step took place twice for some of the small sized samples (25 mm × 20 mm) to investigate the effect of the second cold-pressing cycle on their Joule heating behaviour.

2.3 Fabrication of the large size concept heating device

Fig. S1 (ESI†) depicts the view of the Ecoflex substrate and concept heating device. First, 8 ml of each Ecoflex component was mixed. Next, the mixture was spread into a mould (120 mm × 120 mm) made of poly(methyl methacrylate) or acrylic, until a flat surface was achieved. The mould was then placed in an oven at 80 °C for 45 min. After this step, a 3 × 3 array of CWFs were placed on the Ecoflex layer without any further additives or surface modifications. At this stage, copper tapes as electrodes were carefully placed on top of the electrodes previously attached to the CWFs so that stacks of two layers of copper tape were formed. Long electrodes provided the opportunity to connect the CWFs in series or parallel such that the current passing through each CWF heater was able to be adjusted. It was also possible to locally generate heat by activating an individual or some of the CWF heaters. A fresh Ecoflex mixture (10 ml of each component) was poured on top of the assembly to cover the surface of the CWF heaters, which resulted in a sandwich-structured assembly. At this stage, the tail of copper tape electrodes was carefully kept outside of the viscous Ecoflex. The second curing cycle was conducted under similar conditions to the first cycle. The view of the concept heating device is shown in Fig. S1b (ESI†).

2.4 Characterization

The electrical resistance (R) of the CWFs (80 mm × 20 mm) after drying was measured following our previously reported procedure using a four-point probe method custom-made setup.[4,8,10] A digital caliper was used to carefully measure the thickness (t) and width (W) of each CWF sample. The average of five measurements taken from different locations of each CWF sample was considered as the representative thickness and width for the calculation of electrical conductivity (σ) using $\sigma = L/(t{\cdot}W{\cdot}R)$. In this equation, L is the distance between the inner electrodes of the four-point probe setup (18 mm). The electrical conductivity of each CWF sample was measured five times on different sides and five samples were employed for the measurements. Therefore, the average value of the electrical conductivity of the CWFs was obtained by calculating the average of 25 measurements.

The surface morphology of the CWFs at different stages of the coating process was studied using SEM (HITACHI SU-70) images. In order to understand the chemical composition of the dispersion, EDS was performed on the dried mixture of GNPs/CB/SDBS particles. TGA for the neat and CWF samples was performed using a TA instrument (Q5000 model) in an N_2 atmosphere with an increasing temperature rate of 10 °C min^{-1} up to 600 °C. XRD for the samples was conducted on a Rigaku Ultima IV instrument with a scattering angle, 2θ, ranging from 20° to 80°.

The electrothermal performance of the CWFs was evaluated by the time-dependent surface temperature curves of five different CWF samples for each size. This was conducted by applying different voltages ranging from 2 to 6 V using a power supply (POWERTECH-MP-3086) while the surface temperature at the middle of each CWF sample was recorded using an infrared camera (FLUKE Ti9) every five seconds. The cyclic temperature profile for a CWF sample (25 mm × 20 mm) was obtained during a constant applied voltage for 30 s and naturally cooling down to 30 °C for 10 cycles. In this test, the surface temperature at the middle of the CWF sample was monitored following a similar procedure and settings explained earlier. The experimental setup for these tests is illustrated in Fig. S2 (ESI†).

The performance of the small CWF heaters with a planar area of 25 mm × 20 mm in electrothermal tests indicated their potential applications in large size heating devices that can generate heat with a low input voltage. The electrothermal behaviour of the concept heating device was studied when these CWF heaters were activated either individually or in parallel. A constant voltage was applied to demonstrate the distribution of the surface temperature of the CWF heaters in different modes.

3. Results and discussion

3.1 Fabrication process and characterisation of the CWFs

Fig. 1a schematically shows the steps for the preparation of highly conductive ink based on GNPs and CB particles in DI water using SDBS as a surfactant. Hot-pressed wool fabrics were trimmed to smaller sizes for the stirring process. The trimmed wool fabrics were stirred for 3 min in highly conductive ink, followed by dip coating after drying as the second coating cycle, Fig. 1b. After the second drying cycle, the CWFs were cold-pressed together with copper tape electrodes. The detailed information regarding this process is provided in the Experimental section. The average thickness of the CWFs was measured to be 1.01 ± 0.05 mm. Considering the measured

thickness of the plain weave wool fabric (0.70 ± 0.06 mm), the approximate thickness of the conductive coating on the wool fabrics was about 0.3 mm. Before characterization of the CWF samples, EDS was performed at four random locations on the dried hybrid powder of GNPs/CB/SDBS. As presented in Fig. S3 (ESI†), the elemental composition of the powder was 96.46 ± 1.41, 1.72 ± 0.31, 0.85 ± 0.13 and 0.95 ± 0.31 atomic percentage for C, O, Na and S, respectively. It is obvious that carbon is the dominant element in all locations. The results clearly indicate the presence of SDBS composed of Na, S and O atoms.

SEM images from the surface of the wool fabric and its fibres before the coating process are shown in Fig. 2a and b. After stirring for 3 min, SEM images were taken from the surface of a dried CWF sample, as depicted in Fig. 2c and d. It can be clearly observed that large cracks with large gaps exist on the surface of the CWFs. This deteriorated the electrical conductivity of the CWFs, which is not ideal for the fabrication of heating devices working with a low input voltage. Larger initial resistance leads to larger power consumption as well as larger Joule heating if the current is set to a constant value. In this case, it would also affect the input applied voltage on the CWFs in the beginning of the experiment by the power supply and the applied voltage would have to increase ($V = R.I$). In order to keep the input voltage low, and thus input power low ($P = V.I$), it is desired to have CWFs with low initial resistivity (or lower initial resistance) or high electrical conductivity. Therefore, the second step of the coating was carried out by simple dip coating of the CWFs in the same conductive ink to decrease the level of initial resistance of the CWFs, as suggested in previous studies.[33–35] The SEM images taken after re-coating revealed that the crack gap and its density on the surface of the CWFs decreased, which would lead to a slight increase in their conductivity due to the formation of more connected networks of coated conductive particles, Fig. 2e and f. Removal of the existing surface cracks of the CWFs would lead to the absence of hotspots and achieving a more uniform surface temperature. For this purpose, the CWF samples were cold-pressed under a high compressive load. Fig. 2g and h show the SEM images from the surface of the CWF sample after this step, evidently indicating the removal of surface cracks. In addition, Fig. S4 (ESI†) indicates the homogenous distribution of GNP and CB particles on the conductive layer.

The electrical conductivity of each CWF sample (80 mm × 20 mm) was measured five times using a four-point probe method. The average electrical conductivity of the five CWF samples was found to be 393.04 ± 18.39 S m^{-1} for 25 measurements. The value of electrical conductivity of each sample is depicted in Fig. 2i. It can be seen that the average electrical conductivity of each sample was similar, which indicates the uniformity of the formed percolated networks within the CWFs. The high level of electrical conductivity obtained for CWFs was mainly due to the formation of robust percolated networks of conductive particles after the two coating cycles. The synergistic effect of GNPs and CB on the electrical conductivity of coated natural materials was thoroughly investigated in our previous study.[10] In brief, CB

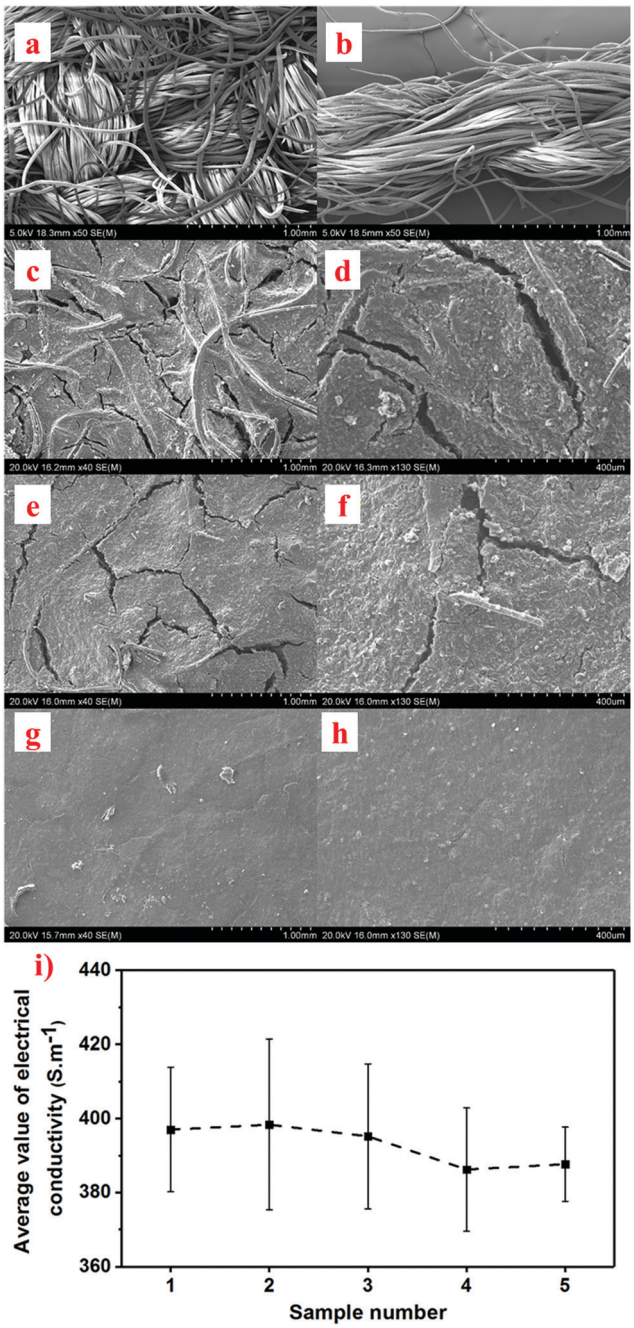

Fig. 2 SEM images from the surface of a CWF sample at different stages of the fabrication process and different magnifications; (a and b) neat wool fabric and its yarn, (c and d) after stir coating, (e and f) after dip coating, and (g and h) after cold-pressing; (i) average value of electrical conductivity for each CWF sample after five measurements.

particles have a large particle size (30 nm) that could bridge the GNPs (5 nm in thickness and 5 μm in width) on the surface of the CWFs, and thus, enhance the level of electrical conductivity. The minimized level of cracks on the surface of the CWFs after the cold-pressing process also played a key role in the improvement of the electrical conductivity of the CWFs.

The XRD spectra of the neat wool and CWFs are presented in Fig. S5 (ESI†). In the case of neat wool, two crystal structures are

typically observed. They are at 2θ = 19.9° and 23.6°, which correspond to α-helix and β-sheet structures, respectively.[31] Compared to the neat wool, the XRD patterns for CWFs clearly show a graphite characteristic peak at 2θ = 26.7° and a peak at about 32.4° related to sodium sulfate. These changes clearly show the presence of SDBS in the conductive layer after the coating process, Fig. S5b (ESI†).

TGA was performed for understanding the decomposition temperature for the wool fabric and CWFs after the second cold-pressing cycle. The TGA graphs in Fig. S6 (ESI†) clearly exhibit an initial weight loss for both neat wool and CWFs due to the evaporation of existing water absorbed from the environment.[36,37] A major weight loss started occurring slightly above 250 °C in both wool and CWFs. Wool fabric exhibited approximately 75% weight loss up to 600 °C while the CWFs had about 65% weight loss at the end of the process. The lower weight loss of CWFs was due to the presence of the hybrid of GNPs and CB particles. Overall, the results showed the thermal stability of the CWFs in the working temperature range of the heaters up to about 250 °C.

3.2 Electrothermal characterisation of the CWF heaters

The time-dependent temperature profiles of five heaters in planar areas of 45 mm × 20 mm and 25 mm × 20 mm at applied voltages within the range of 2–6 V (input power of ~2.3–8.5 W) were obtained. It is worth noting that a trial

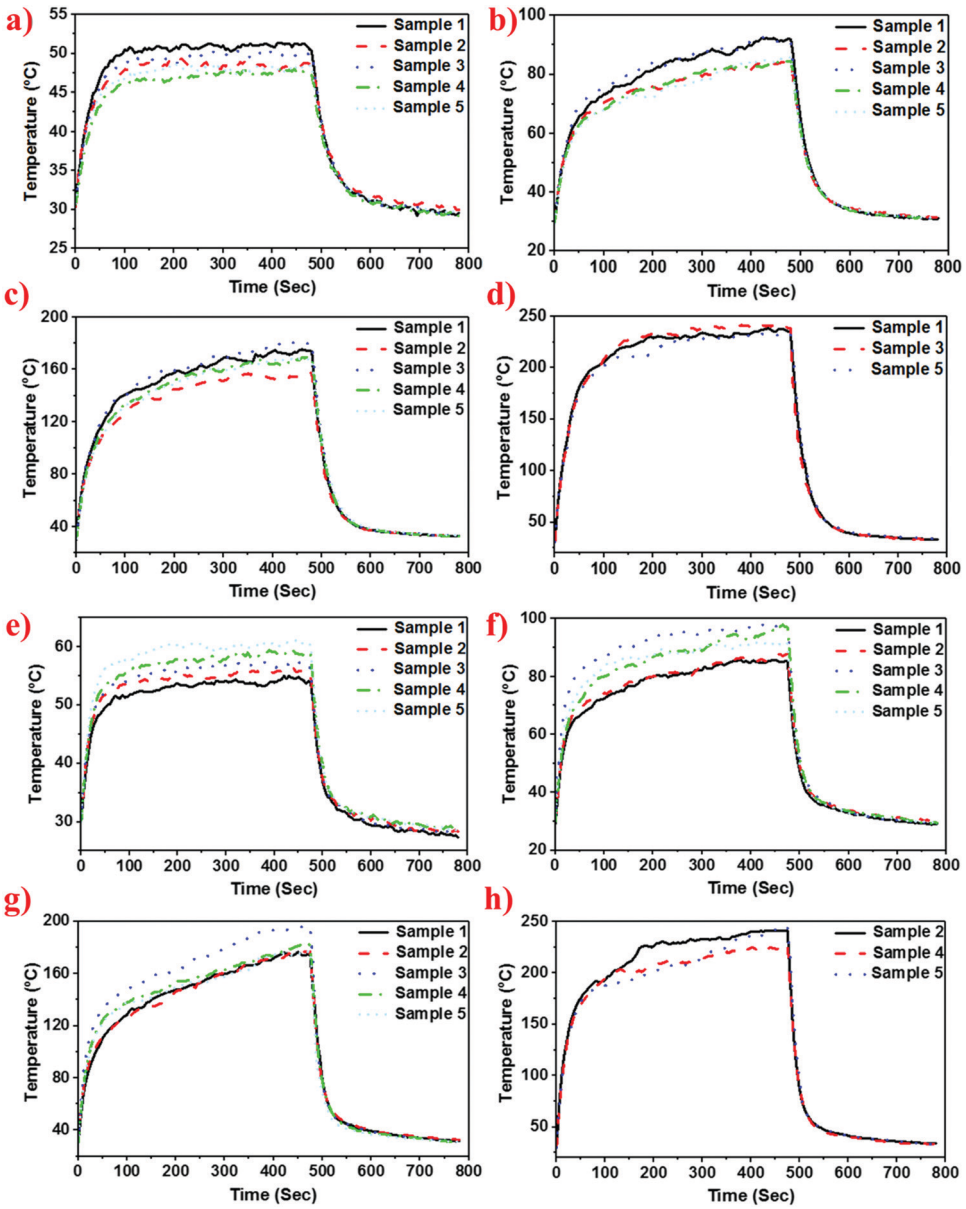

Fig. 3 Time-dependent temperature changes of five large CWF heaters with a planar area of 45 mm × 20 mm at applied voltages of (a) 2 V (~2.5 W), (b) 3.5 V (~4.8 W), (c) 5 V (~6.7 W) and (d) 6 V (~8.5 W), and profiles of small CWF heaters with a planar area of 25 mm × 20 mm at applied voltages of (e) 2 V (~2.3 W), (f) 3 V (~4.1 W), (g) 4 V (~5.8 W), and (h) 4.5 V (~7.2 W).

heating cycle on each sample was performed to increase the temperature on the surface to above 100 °C followed by naturally cooling down to 30 °C. Next, to perform the test, the input voltage was applied for 8 min followed by natural cooling for 5 min. It can be noticed from the time-dependent temperature profiles that they can be divided into three regions: the increasing temperature, steady-state temperature and cooling phase.

Fig. 3a–d show the electrothermal behaviour of the five CWF heaters with a planar area of 45 mm × 20 mm at different applied voltages. It can be observed that all CWF heaters exhibited similar behaviour at a certain applied voltage, indicating the consistency of the proposed process for the fabrication of CWF heaters. As shown in Fig. 3a, a maximum steady-state temperature of 51.4, 49.3, 50.7, 48 and 48.8 °C at an applied voltage of 2 V (~2.5 W) was obtained for CWF heaters 1 to 5, respectively. In addition, the maximum steady-state temperatures of 92.4, 84.3, 92.8, 84.5 and 86.1 °C and 175.4, 158.1, 181.3, 169.8 and 169.3 °C were recorded for CWF heaters 1 to 5 at applied voltages of 3.5 (~4.8 W) and 5 V (~6.7 W), respectively, Fig. 3b and c. Among the five CWF heaters, three high performance heaters in terms of maximum steady-state temperature were chosen to monitor their surface temperature at 6 V (~8.5 W). Based on Fig. 3d, samples 1, 3 and 5 possessed similar temperature profiles with maximum steady-state temperatures of 238.3, 242.7 and 233.8 °C, respectively. The slight differences in the temperature profiles could be due to the slight difference in the initial resistance of the CWF heaters. The results support that the heaters can efficiently generate heat at a low input voltage and work well even at high temperatures (more than 230 °C). The resistance change profile of a large CWF heater *versus* surface temperature is depicted in Fig. S7a (ESI†). The initial resistance between the two electrodes was found to be as low as 4.2 Ω, indicating the high electrical conductivity of the CWF heaters even after the first cold-pressing cycle. The resistance of the CWF heater gradually decreased to about 3.6 Ω as the surface temperature increased to about 230 °C.

Five CWF heaters with a planar area of 25 mm × 20 mm were characterized to compare their electrothermal performances with those of large CWF heaters (45 mm × 20 mm). Overall, the small CWF heaters generated similar surface temperatures with lower input power levels, mainly due to the lower initial resistance between their electrodes, Fig. 3. Similar surface temperature profiles for the CWF samples were observed, as illustrated in Fig. 3e–g. Maximum surface temperatures of 55, 85.8 and 176.4 °C were recorded for the CWF heater 1 when 2 V (~2.3 W), 3 V (~4.1 W) and 4 V (~5.8 W) were applied, respectively. Maximum surface temperatures of 56.3, 57.6, 59.4, and 61.1 °C were recorded for the CWF heaters 2, 3, 4 and 5 at an applied voltage of 2 V (~2.3 W), respectively. In addition, CWF heaters 2, 3, 4 and 5 showed maximum temperatures of 87.9, 98.5, 98, and 92.2 °C with an input voltage of 3 V (~4.1 W) and 176.9, 195.8, 182.9, and 177.5 °C with an input voltage of 4 V (~5.8 W), respectively. Fig. 3h indicates the electrothermal behaviour of three small heaters, chosen based on the maximum steady-state temperature, at 4.5 V (7.2 W) of applied voltage. A great surface temperature was achieved for each of the three small heaters with an average of 238.2 ± 7.2 °C at a lower applied voltage than large CWF heaters. A summary

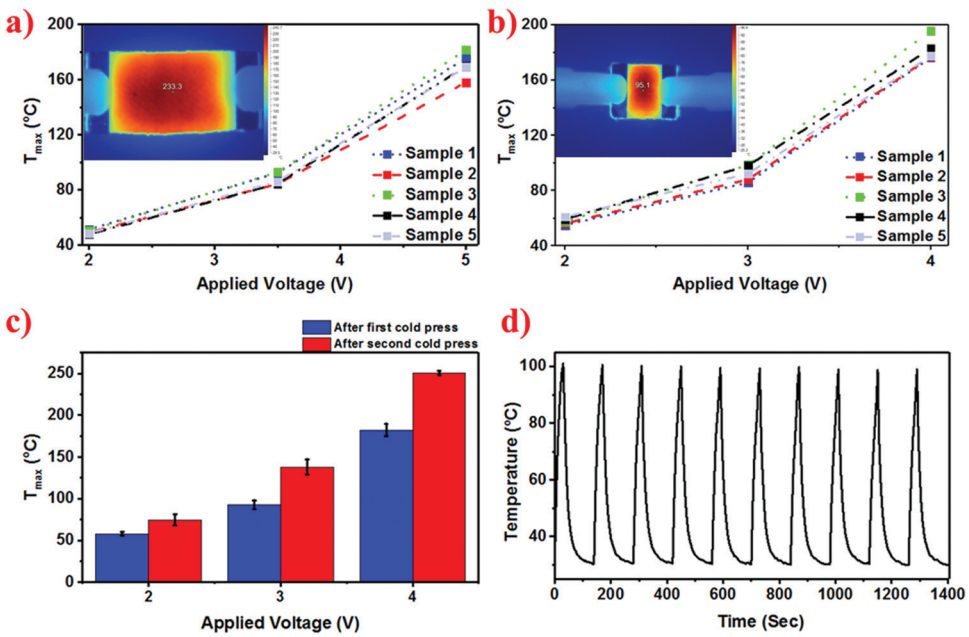

Fig. 4 Maximum surface temperatures for different samples at various applied voltages for (a) large heaters (with a planar area of 45 mm × 20 mm), (b) small heaters (with a planar area of 25 mm × 20 mm) (inset IR image showing the temperature distribution on the surface of a CWF heater in different sizes); (c) comparison of the maximum surface temperature of the small CWF heaters before and after the second cold-pressing, and (d) cyclic electrothermal performance of a small CWF heater at a constant applied voltage of 2.5 V, showing the heating stability of the CWF heaters.

of the maximum surface temperatures for each CWF heater for both sizes at different applied voltages is illustrated in Fig. 4a and b. The maximum generated surface temperature by the CWF heaters is similar, indicating the robust behaviour of the heaters. It is obvious from the results that the small CWF heaters can rapidly reach a high surface temperature with a lower input voltage compared to the larger heaters. Furthermore. the inset of Fig. 4a and b indicates a uniform surface temperature for the heaters without the existence of any hot-spot. These characteristics make them suitable for the application of heating devices. Considering the results, the effect of repeating the cold-pressing step was studied only in small CWF heaters. For this purpose, the previously cold-pressed small CWF heaters were heated in their trial heating cycle and after naturally cooling down, they were cold-pressed for the second time in the same manner as the first cold-pressing cycle.

The maximum surface temperatures of these small CWF heaters during 8 min of applying input voltage were recorded and compared with the results presented in Fig. 4b. The increase in the maximum surface temperature of the small CWF heaters can obviously be noticed in Fig. 4c. The average of the maximum surface temperatures of 74.4 ± 6.8, 138.1 ± 8.9 and 250.7 ± 2.5 °C was found for the small CWF heaters after the second cold-pressing cycle at applied voltages of 2, 3 and 4 V, respectively. This increment of the surface temperature could be due to the lowered contact resistance between the electrodes and the surface of the CWF heaters, as depicted in Fig. S7b (ESI†). Fig. S7b (ESI†) demonstrates the resistance change of a small CWF heater during the Joule heating process. A similar trend was observed compared to the large heater. It is obvious that the initial resistance of the small heaters was lower than that of the large ones (as low as 2.9 Ω). This value decreased further to 2.47 Ω at about 220 °C. The low level of initial resistance of the small CWF heaters after the second cold-pressing process contributed to reaching an even higher surface temperature at an equivalent level of input power compared to the small CWF heater after the first cold-pressing cycle when the initial resistance was approximately 3.4 Ω.

A cyclic electrothermal test on a small CWF heater after the second cold-pressing cycle was conducted at a constant applied voltage of 2.5 V for 10 cycles. The initial temperature of the CWF heater was set to be 30 °C and it was Joule heated for 30 s. Next, the CWF heater was naturally cooled-down to reach 30 °C, which approximately took about 110 s. From there, the next cycles were performed in a similar manner to the first cycle. Fig. 4d exhibits a stable dynamic electrothermal characteristic for the CWF heater with a peak temperature of about 100 °C at each cycle. Overall, it can be said that the electrothermal performance of the CWF heaters outperformed some of the reported heaters based on natural materials, as summarized in Table S1 (ESI†).[22–30]

3.3 Demonstration of the concept of a large size heating device

The electrothermal characterization results of small CWF heaters showed that they are suitable candidates as heating elements for a large size heating device. Therefore, a concept device was designed and fabricated based on a 3 × 3 array of CWF heaters, as depicted in Fig. S1 (ESI†). It was realized that the initial resistance of the CWF heaters increased after being encapsulated by Ecoflex, as a protective layer, which can be due to the addition of the insulating elastomer and its partial penetration into the surface coating of CWF heaters. The electrothermal behaviour of the concept heating device was

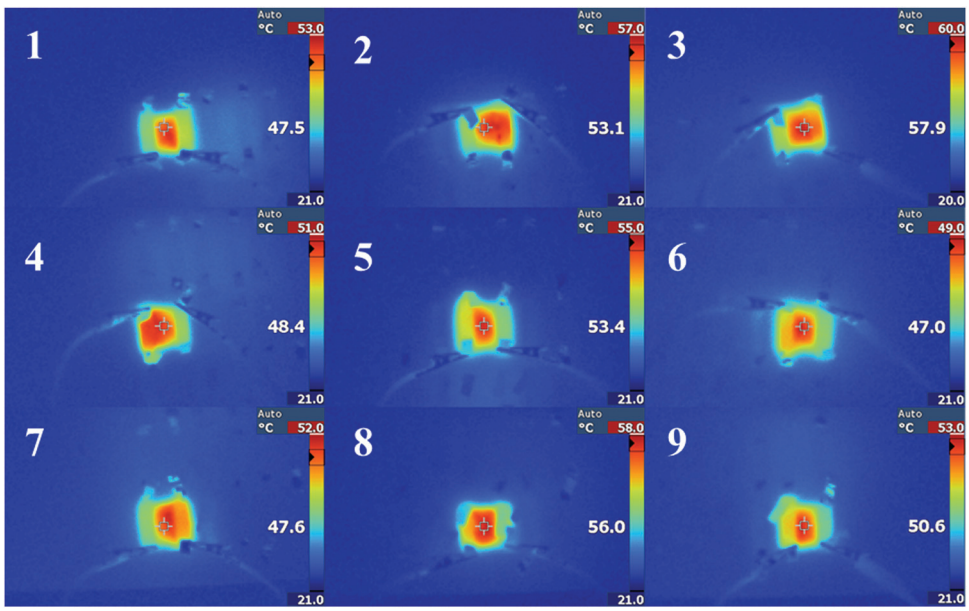

Fig. 5 Steady-state temperature profiles by IR images for CWF heaters 1 to 9 (as numbered in Fig. S1, ESI†) embedded in the device at a constant applied voltage.

characterized by applying a constant voltage (5 V) to each heater until reaching the maximum steady state temperature.

Fig. 5 portrays the CWF heaters embedded in the device when a steady-state temperature was reached. The steady-state temperature on the surface of the demonstrator was found to be 47.5, 53.1, 57.9, 48.4, 53.4, 47.0, 47.6, 56.0 and 50.6 °C corresponding to the CWF heaters 1 to 9 (as numbered in Fig. S1, ESI†), respectively. It was found that the CWF heaters could generate an average temperature of 51.4 ± 4.3 °C on the surface of the demonstrator at an applied voltage of 5 V. The device can also function in different modes by connecting the electrodes of small CWF heaters to activate various numbers of them. For instance, three of the heaters in the left column (number 1, 4 and 7) were linked with each other and activated with 8 V to observe their surface temperature during the Joule heating and cooling processes. Fig. S8 (ESI†) shows the Joule heated CWF heaters connected in parallel, indicating the distribution of surface temperature for each heater, Fig. S8a (ESI†). Fig. S8b (ESI†) shows the surface temperature of the device after being naturally cooled down.

4. Conclusions

In summary, a multi-step process for the fabrication of CWFs using highly conductive ink was introduced, which included stir coating, dip coating and cold-pressing after drying. After this process, the existing cracks within the coated particles were effectively reduced, which resulted in an increase in the electrical conductivity of CWFs with an average of 393.04 ± 18.39 S m^{-1} after the first cold-pressing cycle. CWF heaters in two different sizes (45 mm × 20 mm and 20 mm × 20 mm) were prepared for electrothermal characterization. The electrothermal behaviour of five samples for each size showed a high surface temperature with a low applied voltage. The electrothermal tests of the CWF heaters for large samples were carried out within the range of 2 to 6 V (up to 8.5 W), reaching the maximum surface temperature of up to about 240 °C. Small CWF heaters showed similar maximum temperatures with a lower range of input power (2.3–7.2 W).

The electrothermal performance of the small CWF heaters improved even more after the second cold-pressing cycle as it helped to decrease the contact resistance between the electrodes and the surface of CWFs.

The superior electrothermal performance of the CWF heaters led to a large size concept heating device. The fabricated concept device took advantage of 9 small CWF heaters after two cycles of cold-pressing, positioned in a 3 × 3 array. The steady-state surface temperature profile correlated with each heater and the electrothermal behaviour of the heaters when they were connected in parallel was demonstrated.

Overall, it can be said that the CWF heaters that take advantage of a cost-effective and environmentally friendly fabrication process as well as interesting features such as light weight and low activation voltage could be suitable for large size heating devices for de-icing or warming of complex surfaces (*e.g.* seat heaters). It could also be added that the application of such heating devices could be extended towards wearables by applying design changes (*e.g.* flexible and stretchable electrodes) to better accommodate stretchability. In such wearable applications, future research on the washability of heaters could also be investigated.

Conflicts of interest

The authors declare no conflict of interest.

Acknowledgements

The authors thank staff members and technicians at the Centre for Advanced Composite Materials (CACM) at The University of Auckland, for their assistance. In addition, the authors would like to acknowledge the financial support from the Ministry of Business, Innovation & Employment (MBIE), New Zealand (grant number: UOAX1415).

References

1 H. Souri, H. Banerjee, A. Jusufi, N. Radacsi, A. A. Stokes, I. Park, M. Sitti and M. Amjadi, Wearable and Stretchable Strain Sensors: Materials, Sensing Mechanisms, and Applications, *Adv. Intell. Syst.*, 2020, **2**, 2000039.
2 S. Choi, H. Lee, R. Ghaffari, T. Hyeon and D. H. Kim, Recent Advances in Flexible and Stretchable Bio-Electronic Devices Integrated with Nanomaterials, *Adv. Mater.*, 2016, **28**, 4203–4218.
3 R. F. Service, Technology. Electronic textiles charge ahead, *Science*, 2003, **301**, 909–911.
4 H. Souri and D. Bhattacharyya, Highly Stretchable Multifunctional Wearable Devices Based on Conductive Cotton and Wool Fabrics, *ACS Appl. Mater. Interfaces*, 2018, **10**, 20845–20853.
5 J. Ge, H. Bin Yao, W. Hu, X. F. Yu, Y. X. Yan, L. B. Mao, H. H. Li, S. S. Li and S. H. Yu, Facile dip coating processed graphene/MnO_2 nanostructured sponges as high performance supercapacitor electrodes, *Nano Energy*, 2013, **2**, 505–513.
6 X. Ye, Q. Zhou, C. Jia, Z. Tang, Z. Wan and X. Wu, A Knittable Fibriform Supercapacitor Based on Natural Cotton Thread Coated with Graphene and Carbon Nanoparticles, *Electrochim. Acta*, 2016, **206**, 155–164.
7 H. Souri and D. Bhattacharyya, Highly stretchable and wearable strain sensors using conductive wool yarns with controllable sensitivity, *Sens. Actuators, A*, 2019, **285**, 142–148.
8 H. Souri and D. Bhattacharyya, Electrical conductivity of the graphene nanoplatelets coated natural and synthetic fibres using electrophoretic deposition technique, *Int. J. Smart Nano Mater.*, 2018, **9**, 167–183.
9 X. Zhou, W. Song and G. Zhu, A facile approach for fabricating silica dioxide/reduced graphene oxide coated cotton fabrics with multifunctional properties, *Cellulose*, 2020, **27**, 2927–2938.

10 H. Souri and D. Bhattacharyya, Wearable strain sensors based on electrically conductive natural fiber yarns, *Mater. Des.*, 2018, **154**, 217–227.
11 J. J. Park, W. J. Hyun, S. C. Mun, Y. T. Park and O. O. Park, Highly stretchable and wearable graphene strain sensors with controllable sensitivity for human motion monitoring, *ACS Appl. Mater. Interfaces*, 2015, **7**, 6317–6324.
12 H. Barani, A. Miri and H. Sheibani, Comparative study of electrically conductive cotton fabric prepared through the in situ synthesis of different conductive materials, *Cellulose*, 2021, 1–21.
13 M. A. Kang, S. Ji, S. Kim, C. Y. Park, S. Myung, W. Song, S. S. Lee, J. Lim and K. S. An, Highly sensitive and wearable gas sensors consisting of chemically functionalized graphene oxide assembled on cotton yarn, *RSC Adv.*, 2018, **8**, 11991–11996.
14 Y. Li, Y. Zhang, H. Zhang, T. L. Xing and G. Q. Chen, A facile approach to prepare a flexible sandwich-structured supercapacitor with rGO-coated cotton fabric as electrodes, *RSC Adv.*, 2019, **9**, 4180–4189.
15 Z. Wang, Y. Huang, J. Sun, Y. Huang, H. Hu, R. Jiang, W. Gai, G. Li and C. Zhi, Polyurethane/Cotton/Carbon Nanotubes Core-Spun Yarn as High Reliability Stretchable Strain Sensor for Human Motion Detection, *ACS Appl. Mater. Interfaces*, 2016, **8**, 24837–24843.
16 S. Huang, P. Chen, W. Lin, S. Lyu, G. Chen, X. Yin and W. Chen, Electrodeposition of polypyrrole on carbon nanotube-coated cotton fabrics for all-solid flexible supercapacitor electrodes, *RSC Adv.*, 2016, **6**, 13359–13364.
17 X. Luo, Y. Liang, W. Weng, Z. Hu, Y. Zhang, J. Yang, L. Yang and M. Zhu, Polypyrrole-coated carbon nanotube/cotton hybrid fabric with high areal capacitance for flexible quasi-solid-state supercapacitors, *Energy Storage Mater.*, 2020, **33**, 11–17.
18 L. R. Pahalagedara, I. W. Siriwardane, N. D. Tissera, R. N. Wijesena and K. N. de Silva, Carbon black functionalized stretchable conductive fabrics for wearable heating applications, *RSC Adv.*, 2017, **7**, 19174–19180.
19 Y. Lian, H. Yu, M. Wang, X. Yang, Z. Li, F. Yang, Y. Wang, H. Tai, Y. Liao, J. Wu and X. Wang, A multifunctional wearable E-textile via integrated nanowire-coated fabrics, *J. Mater. Chem. C*, 2020, **8**, 8399–8409.
20 Y. Atwa, N. Maheshwari and I. A. Goldthorpe, Silver nanowire coated threads for electrically conductive textiles, *J. Mater. Chem. C*, 2015, **3**, 3908–3912.
21 Y. Lian, H. Yu, M. Wang, X. Yang and H. Zhang, Ultrasensitive wearable pressure sensors based on silver nanowire-coated fabrics, *Nanoscale Res. Lett.*, 2020, **15**, 1–8.
22 A. Varesano, F. Rombaldoni and C. Tonetti, Electrically conductive and hydrophobic cotton fabrics by polypyrrole-oleic acid coating, *Fibers Polym.*, 2013, **14**, 703–709.
23 S. Lee and C. H. Park, Electric heated cotton fabrics with durable conductivity and self-cleaning properties, *RSC Adv.*, 2018, **8**, 31008–31018.
24 M. Tian, M. Du, L. Qu, K. Zhang, H. Li, S. Zhu and D. Liu, Conductive reduced graphene oxide/MnO_2 carbonized cotton fabrics with enhanced electro -chemical, -heating, and -mechanical properties, *J. Power Sources*, 2016, **326**, 428–437.
25 M. J. Rahman and T. Mieno, Conductive Cotton Textile from Safely Functionalized Carbon Nanotubes, *J. Nanomater.*, 2015, **16**, 187.
26 C. Yeon, G. Kim, J. W. Lim and S. J. Yun, Highly Conductive PEDOT:PSS Treated by Sodium Dodecyl Sulfate for Stretchable Fabric Heaters, *RSC Adv.*, 2017, **7**, 5888.
27 D. Doganay, S. Coskun, S. P. Genlik and H. E. Unalan, Silver nanowire decorated heatable textiles, *Nanotechnology*, 2016, **27**, 435201.
28 M. Zhang, C. Wang, X. Liang, Z. Yin, K. Xia, H. Wang, M. Jian and Y. Zhang, Weft-Knitted Fabric for a Highly Stretchable and Low-Voltage Wearable Heater, *Adv. Electron. Mater.*, 2017, **3**, 1–8.
29 C. Wang, M. Zhang, K. Xia, X. Gong, H. Wang, Z. Yin, B. Guan and Y. Zhang, Intrinsically Stretchable and Conductive Textile by a Scalable Process for Elastic Wearable Electronics, *ACS Appl. Mater. Interfaces*, 2017, **9**, 13331–13338.
30 P. Ilanchezhiyan, A. S. Zakirov, G. M. Kumar, S. U. Yuldashev, H. D. Cho, T. W. Kang and A. T. Mamadalimov, Highly efficient CNT functionalized cotton fabrics for flexible/wearable heating applications, *RSC Adv.*, 2015, **5**, 10697–10702.
31 K. Wang, R. Li, J. H. Ma, Y. K. Jian and J. N. Che, Extracting keratin from wool by using l-cysteine, *Green Chem.*, 2016, **18**, 476–481.
32 H. Souri and D. Bhattacharyya, Highly sensitive, stretchable and wearable strain sensors using fragmented conductive cotton fabric, *J. Mater. Chem. C*, 2018, **6**, 10524–10531.
33 T. A. Kim, S. S. Kim and M. Park, Acid-treated SWCNT/polyurethane nanoweb as a stretchable and transparent Conductor, *RSC Adv.*, 2012, **2**, 10717–10724.
34 E. Y. Jang, T. J. Kang, H. W. Im, D. W. Kim and Y. H. Kim, Single-walled carbon-nanotube networks on large-area glass substrate by the dip-coating method, *Small*, 2008, **4**, 2255–2261.
35 K. Wang, P. Zhao, X. Zhou, H. Wu and Z. Wei, Flexible supercapacitors based on cloth-supported electrodes of conducting polymer nanowire array/SWCNT composites, *J. Mater. Chem.*, 2011, **21**, 16373–16378.
36 I. Jung, D. Dikin, S. Park, W. Cai, S. L. Mielke and R. S. Ruoff, Effect of Water Vapor on Electrical Properties of Individual Reduced Graphene Oxide Sheets, *J. Phys. Chem. C*, 2008, **112**, 20264–20268.
37 H. Souri, S. J. Yu, H. Yeo, M. Goh, J. Y. Hwang, S. M. Kim, B. C. Ku, Y. G. Jeong and N. H. You, A facile method for transparent carbon nanosheets heater based on polyimide, *RSC Adv.*, 2016, **6**, 52509–52517.